CMS Physics Analysis Summary

Contact: cms-pag-conveners-higgs@cern.ch 2018/11/24

Search for an exotic decay of the Higgs boson to a pair of light pseudoscalars with two muons and two b jets in the final state at $\sqrt{s} = 13\,\text{TeV}$

The CMS Collaboration

Abstract

A search for exotic decays of the Higgs boson to a pair of light pseudoscalar particles a_1 is performed under the hypothesis that one of the pseudoscalars decays to a pair of opposite sign muons and the other decays to a $b\bar{b}$ pair. Such signatures are predicted in a number of extensions of the standard model (SM), including next-to-minimal supersymmetry and two-Higgs-doublet models with an additional scalar singlet. A data sample corresponding to an integrated luminosity of $35.9\,\text{fb}^{-1}$ recorded with the CMS detector in 2016 is studied. No statistically significant excess is observed with respect to the SM backgrounds in the search region for pseudoscalar masses from 20 GeV to half of the Higgs boson mass. Upper limits at 95% confidence level are set on the production cross section times branching ratio, $\sigma_h \times \mathcal{B}(h \to a_1 a_1 \to \mu^+\mu^- b\bar{b})$, ranging from 5 to 36 fb, depending on the pseudoscalar mass. Corresponding limits on the branching ratio, assuming the SM prediction for σ_h, are $(1\text{–}6) \times 10^{-4}$.

1 Introduction

The discovery of the particle now identified as the Higgs boson by the ATLAS and CMS experiments [1–3] at the CERN LHC [4] has opened a new era in the history of particle physics. So far, precise measurements of the Higgs boson spin, parity, width, and couplings in production and decay have been consistent with the standard model (SM) Higgs boson [5–9]. However the possibility of exotic Higgs boson decays to new lighter bosons is not excluded. The LHC combination of the SM Higgs boson measurements at 7 and 8 TeV allows Higgs boson decays to states Beyond the SM (BSM) with a rate of up to 34% [7] at 95% confidence level (CL). The LHC data at 13 TeV place an upper limit of 30%–40% for the Higgs boson branching ratio ($\mathcal{B}$) to BSM particles at 95% CL [10, 11].

Several searches for exotic decays of the Higgs boson have been performed at the LHC, using the data at 8 TeV [12–15] and 13 TeV [16–21]. Such decays occur in the context of the next-to-minimal supersymmetric standard model, NMSSM, and extensions to two-Higgs-doublet models (2HDM) where the existence of a scalar singlet is hypothesised (2HDM+S) [22]. The 2HDM, and hence 2HDM+S, are categorised into four types depending on the interaction of SM fermions with the Higgs doublet structure [15]. All SM particles couple to the first Higgs doublet, Φ_1, in type I models. In type II models, up-type quarks couple to Φ_1 while leptons and down-type quarks couple to the second Higgs doublet, Φ_2. Type II models have NMSSM as a special case where the additional singlet is introduced to resolve the μ-problem of the MSSM superpotential [23–25]. Quarks couple to Φ_1 and leptons couple to Φ_2 in type III models. In type IV models, leptons and up-type quarks couple to Φ_1, while down-type quarks couple to Φ_2. After electroweak symmetry breaking, the 2HDM predicts a pair of charged Higgs bosons $\mathrm{H}^{\pm}$, a neutral pseudoscalar A, and two neutral scalar mass eigenstates, H and h. In the decoupling limit the lighter scalar eigenstate, h, is the observed boson with $m_{\mathrm{h}} \approx 125$ GeV. In 2HDM+S models, a complex scalar singlet $S_{\mathrm{R}} + iS_{\mathrm{I}}$ is introduced that has no direct Yukawa couplings. Hence, it is expected to decay to SM fermions by virtue of mixing with the Higgs sector. This mixing is small enough to preserve the SM-like nature of the h boson.

In this note we consider the Higgs boson decay to a pair of a_1 particles where a_1 is a pseudoscalar mass eigenstate mostly composed of S_{I}. We perform a search for the final state $\mathrm{h} \to \mathrm{a}_1\mathrm{a}_1 \to \mu^+\mu^-\mathrm{b\bar{b}}$. The gluon gluon fusion (ggF) and the vector boson fusion (VBF) production mechanisms are considered with production cross sections $\sigma^{\mathrm{N3LO}}_{\mathrm{gg}\to\mathrm{h}} = 48.58 \pm 1.89\,\mathrm{pb}$ and $\sigma^{\mathrm{NNLO}}_{\mathrm{qq}\to\mathrm{h}} = 3.93 \pm 0.08\,\mathrm{pb}$, respectively [26]. As a benchmark, the branching ratio of $\mathrm{h} \to \mathrm{a}_1\mathrm{a}_1$ is assumed to be 10%. The branching ratios of a_1 to SM particles depend on the type of 2HDM+S, on the pseudoscalar mass m_{a_1}, and on $\tan\beta$, defined as the ratio of the vacuum expectation values of the second and first doublets. The $\tan\beta$ is assumed to be 2 which implies $2 \times \mathcal{B}(\mathrm{a}_1 \to \mathrm{b\bar{b}})\mathcal{B}(\mathrm{a}_1 \to \mu^+\mu^-) = 1.7 \times 10^{-3}$ for $m_{\mathrm{a}_1} = 30\,\mathrm{GeV}$ in type-III 2HDM+S [22]. For the set of parameters under discussion and with $20 < m_{\mathrm{a}_1} < 62.5\,\mathrm{GeV}$, no strong dependence on m_{a_1} is expected for $\mathcal{B}(\mathrm{a}_1 \to \mathrm{b\bar{b}})$ and $\mathcal{B}(\mathrm{a}_1 \to \mu^+\mu^-)$ [22]. The product of the cross section and branching ratio is therefore approximated to be about 7 fb for all m_{a_1} values considered in this analysis.

The present search for the exotic a_1 particle in the $\mu^+\mu^-\mathrm{b\bar{b}}$ final state is sensitive to the mass range of $20 \leq m_{\mathrm{a}_1} \leq 62.5$ GeV. The sensitivity of the search largely decreases towards $m_{\mathrm{a}_1} \approx 20$ GeV and lower because a_1 gets boosted and the two b quark jets tend to merge [27]. The upper bound is imposed by the Higgs boson mass. The analysis is performed using the proton-proton collision data collected with the CMS detector during 2016, corresponding to an integrated luminosity of $35.9\,\mathrm{fb}^{-1}$. The signal selection is optimised for the $\mathrm{h} \to \mathrm{a}_1\mathrm{a}_1 \to \mu^+\mu^-\mathrm{b\bar{b}}$ process. Decays of $\mathrm{h} \to \mathrm{a}_1\mathrm{a}_1 \to \mu^+\mu^-\tau^+\tau^-$ can contribute to the selected sample if hadroni-

cally decaying τ leptons are misidentified as b quark jets. Such a contribution is found to be negligible using the benchmark scenario, although in some parts of the parameter space the enhancement in $\mathcal{B}(a_1 \to \tau^+\tau^-)$ can lead to a nonnegligible fraction of these events surviving the selection. This is taken into account in the scan over the $(m_{a_1}, \tan\beta)$ plane in the type III 2HDM+S, as for certain values, the increase in $\mu^+\mu^-\tau^+\tau^-$ signal can affect the sensitivity. The signal from $a_1a_1 \to b\bar{b}\tau^+\tau^-$ with $\tau \to \mu$ leads to $m_{\mu\mu}$ significantly smaller than m_{a_1} and is not considered in the search.

A similar search from the CMS collaboration in Run I using the 2012 LHC data led to an upper limit of $\mathcal{B}(h \to \mu^+\mu^- b\bar{b}) < 9 \times 10^{-4}$ [15], considering the ggF Higgs production and the mass range $25 \leq m_{a_1} \leq 62.5$ GeV. At 13 TeV, the ggF Higgs production cross section has increased by a factor of about 2.3 over that at 8 TeV, while the production cross section of main backgrounds, Drell–Yan and $t\bar{t}$, has increased by a factor of 1.5 and 3.3, respectively. Despite the relative increase in backgrounds, better sensitivity is achieved using improved analysis techniques in Run II.

2 Simulated samples

The NMSSMHET model [22] is used to generate signal samples with the Monte Carlo (MC) event generator MADGRAPH5_aMC@NLO [28] at leading order (LO). Background processes with dominant contributions are the Drell–Yan production in association with additional b jets and $t\bar{t}$ in the dimuon final state. Simulated samples for background processes are used in this analysis to optimise the selection and for validation purposes in those selection steps that yield reasonable statistical precision. The contribution of backgrounds to the selected sample is directly extracted from data with no reference to simulation. The Drell–Yan process, $Z/\gamma^*(\to \ell^+\ell^-)$ + jets with a minimum dilepton mass threshold of 10 GeV, is modelled with the same event generator at LO, exclusive in number of additional partons (up to 4). The reference cross section for the Drell–Yan process is computed using FEWZ 3.1 [29] at next-to-next-to-leading order. The top quark samples, $t\bar{t}$ and single top quark production, are produced with POWHEG2.0 [30–33] at next-to-leading order (NLO). Backgrounds from diboson (WW, WZ, ZZ) production are generated at NLO with the same program and settings as that of the Drell–Yan samples. The only exception is the WW process that is generated at LO. The set of parton distribution functions (PDFs) is NLO NNPDF3.0 for NLO samples, and LO NNPDF3.0 for LO samples [34]. For all samples, PYTHIA 8.212 [35] with tune CUETP8M1 [36, 37] is used for the modelling of the parton showering and fragmentation. The full CMS detector simulation based on GEANT4 [38] is implemented for all generated event samples. In order to model the effect of additional interactions per bunch crossing (pileup), generated minimum bias events are added to the simulated samples. The number of additional interactions are scaled to agree with that observed in data [39].

3 Event selection and categorisation

Events are filtered using a high-level trigger requirement based on the presence of two muons with $p_T > 17$ and 8 GeV. For offline selection, events must contain at least one primary vertex, considered as the vertex of the hard interaction. At least four tracks must be associated with the selected primary vertex. The longitudinal and radial distances of the vertex from the centre of the detector must be smaller than 24 and 2 cm, respectively. The vertex with the largest sum of p_T^2 of the physics objects is chosen for the analysis. The physics objects are the jets, clustered using the jet finding algorithm [40, 41] with the tracks assigned to the vertex as inputs, and

the associated missing transverse momentum, taken as the negative vector sum of the p_T of those jets. Extra selection criteria are applied to leptons and jets, reconstructed using the CMS particle-flow algorithm [42].

The selection requires two muons with opposite electric charge in $|\eta| < 2.4$, originating from the selected primary vertex. Events with the leading (subleading) muon p_T greater than 20 (9) GeV are selected. An relative isolation variable I_{rel} is calculated by summing the transverse energy deposited by other particles inside a cone of size $\Delta R = \sqrt{(\Delta\eta)^2 + (\Delta\phi)^2} = 0.4$ around the muon with ϕ being the azimuthal angle measured in radians, divided by the muon p_T,

$$I_{rel} = \frac{I^{ch.\,h} + \max((I^{\gamma} + I^{n.\,h} - 0.5 \times I^{PU\ ch.\ h}), 0)}{p_T}, \quad (1)$$

where $I^{ch.\,h}$, I^{γ}, $I^{n.\,h}$ and $I^{PU\ ch.\ h}$ are, respectively, the scalar p_T sums of stable charged hadrons, photons, neutral hadrons, and charged hadrons associated with pileup vertices. The contribution $0.5 \times I^{PU\ ch.\ h}$ accounts for the expected pileup contribution from neutral particles. The neutral-to-charged particle ratio is taken to be approximately 0.5 from isospin invariance. Only muons with the isolation variable satisfying $I_{rel} < 0.15$ are considered in the analysis. The efficiencies for muon trigger, reconstruction, and selection in simulated events are corrected to match those in data. In case more muons in the event pass the selection requirements, the two with the largest p_T are chosen.

Jets are reconstructed by clustering charged and neutral particles using the anti-k_T algorithm [40] with a distance parameter of 0.4. The reconstructed jet energy is corrected for effects from the detector response as a function of the jet p_T and η. Contamination from pileup, underlying event, and electronic noise are subtracted [43, 44]. Extra η-dependent smearing is performed on the jet energy in simulated events as prescribed in Refs. [43, 44].

Events are required to have at least two jets with $|\eta| < 2.4$ and $p_T > 20$ (leading) and 15 GeV (subleading), with both jets separated from the selected muons ($\Delta R > 0.5$). A combined secondary vertex algorithm is used to identify jets that are likely to originate from a b quark. The algorithm uses the track-based lifetime information together with the secondary vertices inside the jet to provide a multivariate discriminator for the b jet identification [45]. Working points "loose" (L), "medium" (M), and "tight" (T) are defined. They correspond to thresholds on the discriminator, for which the misidentification probability is around 10%, 1%, and 0.1%, respectively, for jets originating from light quarks and gluons [45]. The efficiencies for correctly identifying b jets are ≈80% for the loose, ≈60% for the medium, and ≈40% for the tight working point. The jet with maximum discriminator value must pass the tight working point of the algorithm, while the second is required to pass the loose one. The correction factors for b jet identification are applied to simulated events to reproduce the data distribution of the b tagging discriminator. In events with more jets passing the selection criteria, the two with the largest p_T are taken.

The imbalance in the transverse momentum in signal events is not expected to be large, as the contribution from neutrinos from semileptonic decays in b jets is typically small. The missing transverse momentum, p_T^{miss} is defined as the magnitude of the negative vector sum of the transverse momenta of all reconstructed particles. The jet energy calibration therefore introduces corrections to the p_T^{miss} measurement [44]. Events are required to have $p_T^{miss} < 60$ GeV.

Assuming the b quark jets and muons are the decay products of the pseudoscalar a_1, it is expected to have $m_{bb} \approx m_{\mu\mu} \approx m_{a_1}$ in signal events. Moreover, the system of muons and b quark jets is expected to have an invariant mass close to 125 GeV. A χ^2 variable is introduced as

$\chi^2_{\mathrm{bb}} + \chi^2_{\mathrm{h}}$, where

$$\chi_{\mathrm{bb}} = \frac{(m_{\mathrm{bb}} - m_{\mu\mu})}{\sigma_{\mathrm{bb}}} \quad \text{and} \quad \chi_{\mathrm{h}} = \frac{(m_{\mu\mu\mathrm{bb}} - 125)}{\sigma_{\mathrm{h}}}. \tag{2}$$

Here σ_{bb} and σ_{h} are, respectively, the mass resolutions of the di-b-quark jet system and the Higgs boson candidate, derived from simulation. The mass resolution of the di-b-quark jet system increases linearly with m_{a_1}. It is evaluated on an event-by-event basis, where $m_{\mu\mu}$ is assumed to be equal to m_{a_1}. Events are selected with $\chi^2 < 5$. In Fig. 1, χ_{bb} and χ_{h} are shown in 2D histograms for backgrounds and for the signal with $m_{\mathrm{a}_1} = 40$ GeV, where the contour of $\chi^2 < 5$ is also presented. This selection has a signal efficiency up to 64% while rejecting more than 95% of backgrounds. Events with $m_{\mu\mu}$ values not in $[20, 62.5]$ GeV are discarded.

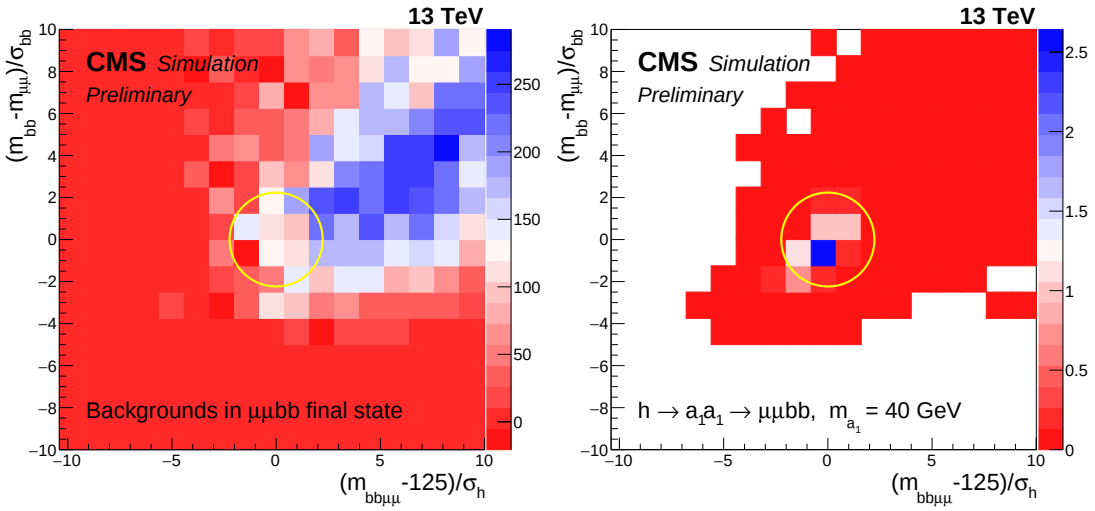

Figure 1: The distribution of χ_{bb} versus χ_{h} as defined in Eq. (2) for (left) simulated background processes and (right) the signal process with $m_{\mathrm{a}_1} = 40$ GeV. The contours encircle the area with $\chi^2 < 5$.

A method that fully relies on data is used to estimate the background. Simulated background samples are however used to optimise the selection. Figure 2 shows distributions, in data and simulation, for events passing the selection requirements except those of $p_{\mathrm{T}}^{\mathrm{miss}}$ and χ^2. In this figure, data and simulation are compared for the p_{T} of the dimuon system, and the mass and p_{T} of the di-b-jet system. Using the same selected muon and jet pairs, Fig. 2 also illustrates the distributions of the invariant mass $m_{\mu\mu\mathrm{bb}}$ and the transverse momentum $p_{\mathrm{T}}^{\mu\mu\mathrm{bb}}$ of the four-body system. The distributions for simulated events follow reasonably those in the data, within the statistical uncertainties presented in the figure. The yields in data and simulation are presented in Table 1. The expected yield from a signal of $\mathrm{h} \to \mathrm{a}_1\mathrm{a}_1 \to \mu^+\mu^-\tau^+\tau^-$ is found to be around 0.01 with the model parameters used in this table.

To enhance the sensitivity, an event categorisation is employed: different categorisation schemes are tried, and the one resulting in the highest expected significance is chosen. The data in a control region are used to model the backgrounds for these sensitivity studies. The control region is constructed using the same selection as that for the signal region except that $5 < \chi^2 < 11$. In simulated background samples, the correlations between χ^2 and $m_{\mu\mu}$ and the variables used for categorisation are found to be small. The best sensitivity is found with categorisation according to the btagging discriminator value of the loose b-tagged jet. The tight-tight (TT) category contains events with both jets passing the tight requirements of the b jet identification algorithm.

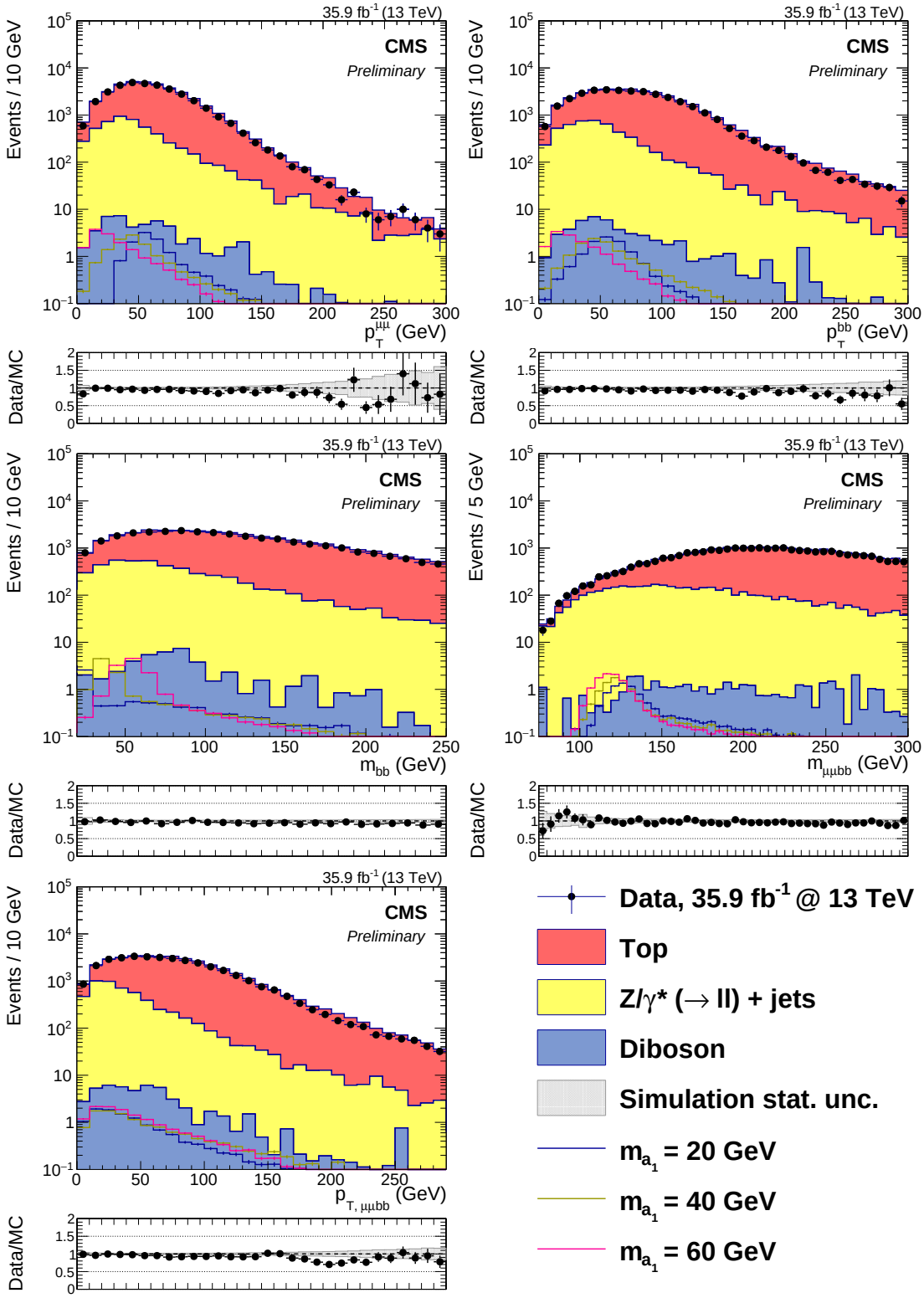

Figure 2: The distribution of the p_{T} of the (top left) dimuon and (top right) di-b-jet system, the mass of the (middle left) di-b-jet and (middle right) $\mu\mu$bb system, and (bottom left) the p_{T} of the $\mu\mu$bb system, all after requiring two muons and two b-tagged jets in the event. Simulated samples are normalised to an integrated luminosity of 35.9 fb^{-1} using their theoretical cross sections.

Table 1: Event yields for simulated processes and data after requiring two muons and two b jets ($\mu^+\mu^-\mathrm{b\bar{b}}$ selection) and after the final selection. The expected number of simulated events is normalised to the integrated luminosity of 35.9 fb^{-1}. Uncertainties are only statistical.

Process	$\mu^+\mu^-\mathrm{b\bar{b}}$ selection	Final selection
Top ($\mathrm{t\bar{t}}$, single top quark)	33730 ± 120	198 ± 9
Drell–Yan	5237 ± 77	399 ± 21
Diboson	51 ± 4	1 ± 0.1
Total expected background	39015 ± 140	598 ± 23
Data	36360	610
Signal for $\sigma_\mathrm{h} \times \mathcal{B} \approx 8$ fb		
$m_{\mathrm{a}_1} = 20$ GeV	14.0 ± 0.1	6.0 ± 0.1
$m_{\mathrm{a}_1} = 40$ GeV	14.8 ± 0.1	7.5 ± 0.1
$m_{\mathrm{a}_1} = 60$ GeV	16.7 ± 0.1	10.1 ± 0.1

Events in which the loose b-tagged jet passes the medium btagging requirements but fails the tight conditions fall into the tight-medium (TM) category. The remaining events with the loose b-tagged jet failing the medium requirements of the b jet identification algorithm belong to the tight-loose (TL) category. On average, 41% of signal events pass the TL selection, while 32% fulfil the TM requirements and 27% belong to the TT category. According to the data in the control region, the majority of background events (≈70%) fall into the TL category whereas about 20% pass the TM requirements and less than 10% can meet the TT criteria.

4 Signal and background modelling

The search is performed using an unbinned fit to the $m_{\mu\mu}$ distribution in data. The signal shape is modelled with a weighted sum of Voigt profile [46] and Crystal Ball (CB) functions [47], where the mean values of the two are bound to be the same. All parameters in the signal model are found to be independent of m_{a_1}, except for the resolution parameter of the Voigt profile and CB functions, σ_v and σ_cb, respectively. These parameters depend linearly on m_{a_1} and only their slopes, respectively α and β, float in the final fit within their uncertainties,

$$\begin{aligned} \sigma_\mathrm{v} &= \sigma_{\mathrm{v},0} + \alpha\, m_{\mu\mu}, \\ \sigma_\mathrm{cb} &= \sigma_{\mathrm{cb},0} + \beta\, m_{\mu\mu}. \end{aligned} \tag{3}$$

The $m_{\mu\mu}$ distribution in data is used to evaluate the contribution of backgrounds. The uncertainty associated with the choice of the background model is treated in a similar way as other uncertainties for which there are nuisance parameters in the fit. The unbinned likelihood function for the signal-plus-background fit has the form

$$\mathcal{L}(\mathrm{data}|s(p, m_{\mu\mu}) + b(m_{\mu\mu})), \tag{4}$$

where $s(p, m_{\mu\mu})$ is the parametric signal shape with the set of parameters indicated by p, and $b(m_{\mu\mu})$ is the background model. The shape for the background is modelled with a set of analytical functions using the discrete profiling method [48–50]. In this approach the choice of the functional form of the background shape is considered as a discrete nuisance parameter, for which the best fit value can vary as the trial value of the parameter of interest ($m_{\mu\mu}$) varies. The background parameter space therefore contains multiple models, each including its own parameters.

To provide the input background models to the discrete profiling method, the data are modelled with different parametrisations of polynomials. The degrees of the polynomials are de-

termined through statistical tests (F-test) [51] to ensure the sufficiency of number of parameters and to avoid over-fitting the data.

The input background functions are tried in the minimisation of the negative logarithm of the likelihood with a penalty term added to account for the number of free parameters in the background model. The likelihood ratio for the penalised likelihood function $\widetilde{\mathcal{L}}$ can be written as

$$-2\ln\frac{\widetilde{\mathcal{L}}(\text{data}|\mu,\hat{\theta}_\mu,\hat{b}_\mu)}{\widetilde{\mathcal{L}}(\text{data}|\hat{\mu},\hat{\theta},\hat{b})}, \tag{5}$$

where μ is the measured quantity. The numerator is the maximum penalised likelihood for a given μ, at the best fit values of nuisance parameters, $\hat{\theta}_\mu$ and of the background function, $\hat{b}_\mu$. The denominator is the global maximum for $\widetilde{\mathcal{L}}$, achieved at $\mu = \hat{\mu}$, $\theta = \hat{\theta}$ and $b = \hat{b}$. A confidence interval for μ is obtained with the background function maximising $\widetilde{\mathcal{L}}$ for any value of μ [48].

5 Systematic uncertainties

The statistical interpretation of the analysis takes into account several sources of systematic uncertainties related to the accuracy in the signal modelling, uncertainties in the signal acceptance, and the imprecise knowledge of the shape of the background contributions, as discussed in Section 4.

Theoretical uncertainties: to evaluate the upper limit on $\mathcal{B}(\mathrm{h} \to \mathrm{a_1a_1} \to \mu^+\mu^-\mathrm{b\bar{b}})$, the Higgs boson production cross section is set to the SM prediction where an uncertainty of 3.6% is considered for the sum of the ggF and VBF production cross sections, accounting for PDF and α_s uncertainties [26].

Uncertainties in signal shape and acceptance modelling: an uncertainty of 2.5% is assigned to the integrated luminosity of the CMS 13 TeV data collected in 2016 [39]. The uncertainty in the number of pileup interactions per event is estimated by varying the total inelastic ppcross section by $\pm$4.6% [52]. The simulation-to-data correction factors for the trigger efficiency, muon reconstruction, and selection efficiencies are estimated using a "tag-and-probe" method [53] in Drell–Yan data and simulated samples. These uncertainties include the pileup dependence of the correction factors. For the jet energy scale (JES), the variations are made according to the η- and p_T-dependent uncertainties and propagated to the $p_\mathrm{T}^\mathrm{miss}$ of the event. An additional uncertainty, arising from unclustered energies in the event, is assessed for $p_\mathrm{T}^\mathrm{miss}$. For the jet energy resolution, the smearing corrections are varied within their uncertainties [43]. Systematic uncertainty sources that affect the simulation-to-data corrections of the b tagging discriminator distribution are JES, the contaminations from light flavor (LF) jets in the b-jet sample, the contaminations from heavy flavor (HF) jets in the light-flavor jet sample, and the statistical fluctuations in data and MC. The uncertainties due to JES and light-flavor jet contamination in b-jet samples are found to be dominant [45]. Finally, uncertainties arising from the limited understanding of the PDFs [54] are taken into account. These uncertainties have a negligible effect on the shape of the signal. Their effects on the yield are taken into account by introducing nuisance parameters with log-normal distributions into the fit.

6 Results

The analysis yields no significant excess of events over the SM background prediction. Figure 3 shows the $m_{\mu\mu}$ distribution in the data of all categories together with the best fit output for the background model, including uncertainties.

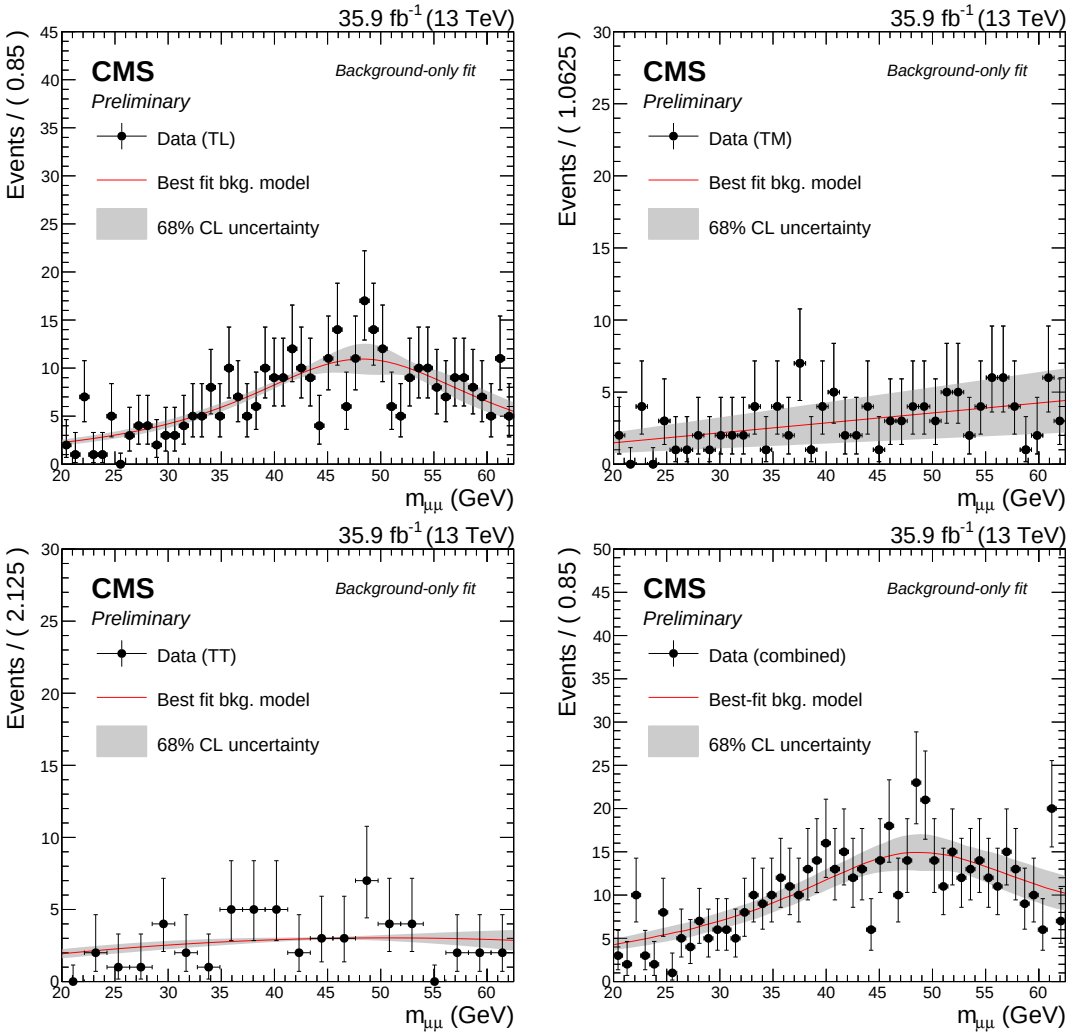

Figure 3: The best fit output to the data under the background-only hypothesis for the (top-left) TL category, (top right) TM category, (bottom left) TT category and (bottom right) all categories, presented together with 68% CL uncertainty band for the background model.

The upper limit on $\sigma_h \times \mathcal{B}(h \to a_1 a_1 \to \mu^+\mu^- b\bar{b})$ is obtained at 95% CL using the CL_s criterion [55, 56] and an asymptotic approximation to the distribution of the profiled likelihood ratio test statistic [57]. Assuming the SM cross sections for the Higgs boson production processes within the theory uncertainties, an upper limit is placed on $\mathcal{B}(h \to a_1 a_1 \to \mu^+\mu^- b\bar{b})$ using the same procedure. Limits are evaluated as a function of m_{a_1}. The observed and expected limits are illustrated in Fig. 4 for both scenarios. Dominant systematic uncertainties are those associated with the b jet identification. For $m_{a_1} = 40$ GeV, the b-tagging uncertainties arising from LF contamination and JES amount to 17% and 14%, respectively. At the same m_{a_1}, the relative difference between the expected limit of the best-fit background model and that of the unconditional fit is about 10%. Other uncertainties are below 5%.

Observed limits on $\mathcal{B}(h \to a_1 a_1)$ are shown in Fig. 5 in the plane of $(m_{a_1}, \tan\beta)$ for type-III and

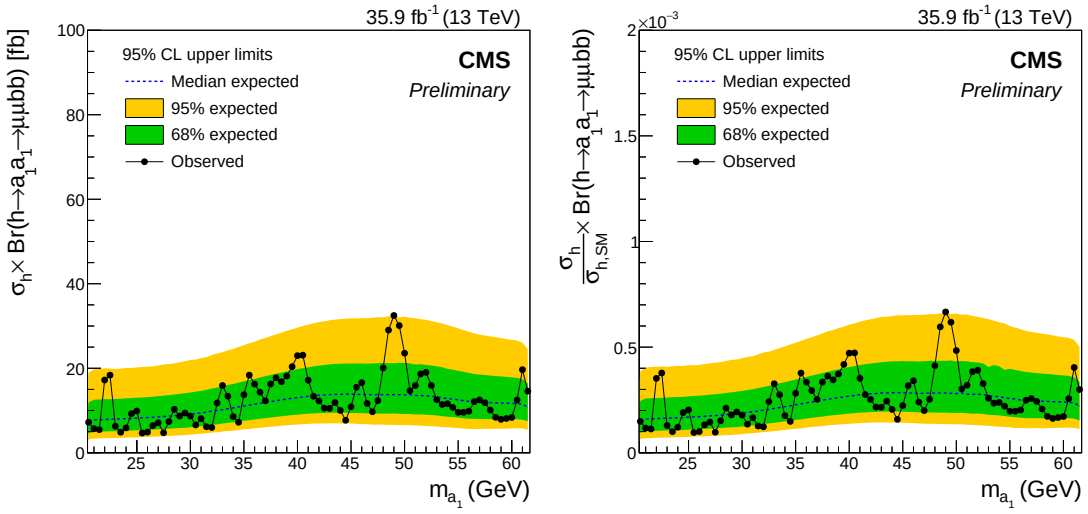

Figure 4: Observed and expected upper limits at 95% CL on the (left) Higgs boson production times $\mathcal{B}(\mathrm{h} \to \mathrm{a_1 a_1} \to \mu^+\mu^-\mathrm{b\bar{b}})$ and (right) the branching ratio as a function of $m_{\mathrm{a_1}}$. The inner and outer bands indicate the regions containing the distribution of limits located within 68% and 95% confidence intervals, respectively, of the expectation under the background–only hypothesis.

type-IV 2HDM+S, using only the $\mu^+\mu^-\mathrm{b\bar{b}}$ signal. The allowed ranges for $\mathcal{B}(\mathrm{h} \to \mathrm{a_1 a_1}) \leq 1$ and $\mathcal{B}(\mathrm{h} \to \mathrm{a_1 a_1}) \leq 0.34$ are also presented. Constraints from Run I Higgs boson measurements at the LHC allow $\mathcal{B}(\mathrm{h} \to \mathrm{BSM})$ up to 0.34 [7].

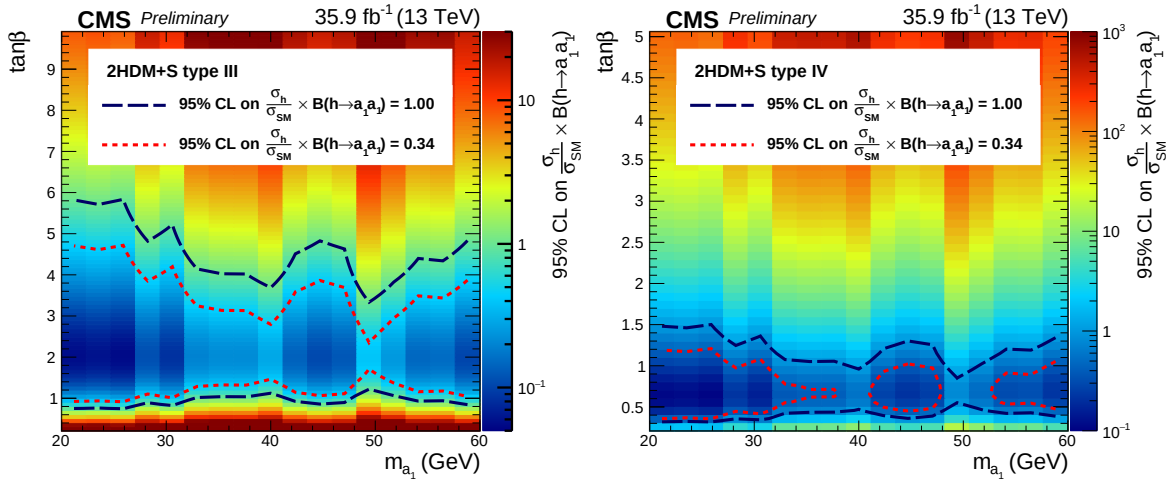

Figure 5: Observed upper limits on $\mathcal{B}(\mathrm{h} \to \mathrm{a_1 a_1})$ in the plane of $(m_{\mathrm{a_1}}, \tan\beta)$ for (left) type-III and (right) type-IV 2HDM+S, using only the $\mu^+\mu^-\mathrm{b\bar{b}}$ signal.

The effect of including the $\mu^+\mu^-\tau^+\tau^-$ signal is studied in the $(m_{\mathrm{a_1}}, \tan\beta)$ plane for the four types of 2HDM+S. For a given $(m_{\mathrm{a_1}}, \tan\beta)$ the relevance of $\mu^+\mu^-\tau^+\tau^-$ depends on the ratio $\mathcal{B}(\mathrm{a_1} \to \tau\tau)\epsilon^{\mathrm{sel.}}_{\mu\mu\tau\tau} / \mathcal{B}(\mathrm{a_1} \to \mathrm{bb})\epsilon^{\mathrm{sel.}}_{\mu\mu\mathrm{bb}}$ as well as the sensitivity of the analysis. Here $\epsilon^{\mathrm{sel.}}$ refers to the acceptance and the selection efficiency of the process. The contribution of the $\mu^+\mu^-\tau^+\tau^-$ signal is found nonnegligible in the type-III 2HDM+S with $\tan\beta \approx 5$. Figure 6 shows the observed limits on $\mathcal{B}(\mathrm{h} \to \mathrm{a_1 a_1})$ in the $(m_{\mathrm{a_1}}, \tan\beta)$ plane, including the contribution of $\mu^+\mu^-\tau^+\tau^-$ signal for type-III 2HDM+S. The observed limit contours of $\mathcal{B}(\mathrm{h} \to \mathrm{a_1 a_1}) = 1.00$ and $\mathcal{B}(\mathrm{h} \to \mathrm{a_1 a_1}) = 0.34$ are extended compared with Fig. 5 (top).

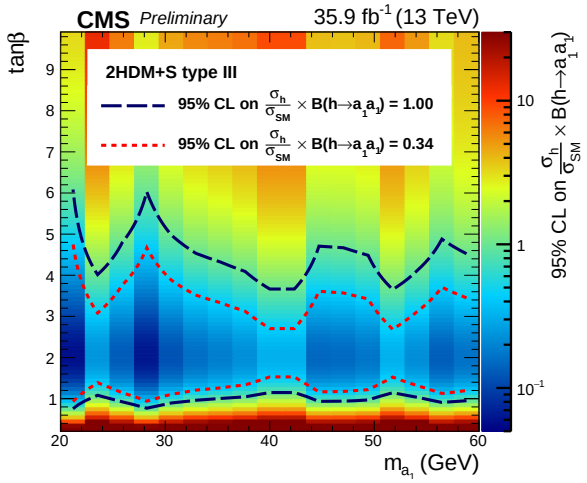

Figure 6: Observed upper limits on $\mathcal{B}(\mathrm{h} \to \mathrm{a_1 a_1})$ in the plane of $(m_{\mathrm{a_1}}, \tan\beta)$ for type-III 2HDM+S, including $\mu^+\mu^-\tau^+\tau^-$ signal that is misidentified as $\mu^+\mu^-\mathrm{b\bar{b}}$.

7 Summary

A search for the Higgs boson decay to a pair of new pseudoscalars $\mathrm{h} \to \mathrm{a_1 a_1} \to \mu^+\mu^-\mathrm{b\bar{b}}$, motivated by the NMSSM and extensions to two-Higgs-doublet models, is carried out using a sample of proton-proton collision data corresponding to an integrated luminosity of 35.9 fb^{-1} at $\sqrt{s} = 13$ TeV. No statistically significant excess is found in data with respect to the SM background prediction. The results of the analysis are presented in the form of upper limits, at 95% CL, on the Higgs boson production cross section times branching ration, $\sigma_{\mathrm{h}} \times \mathcal{B}(\mathrm{h} \to \mathrm{a_1 a_1} \to \mu^+\mu^-\mathrm{b\bar{b}})$ as well as on the Higgs boson branching ratio assuming the SM prediction of σ_{h}. The former ranges between 5 to 36 fb, depending on $\mathrm{m_{a_1}}$. The corresponding limits on the branching ratio are $(1\text{–}6) \times 10^{-4}$ for the mass range of $20 \leq m_{\mathrm{a_1}} \leq 62.5$ GeV. In an analysis performed by ATLAS [19], the limits on the branching ratio range between 2×10^{-4} and 10^{-3}. Compared with the similar analysis in Run I [15], the expected upper limits on the branching ratio are improved by more than a factor of two.

References

[1] ATLAS Collaboration, "Observation of a new particle in the search for the standard model Higgs boson with the ATLAS detector at the LHC", *Phys. Lett. B* **716** (2012) 1, doi:10.1016/j.physletb.2012.08.020, arXiv:1207.7214.

[2] CMS Collaboration, "Observation of a new boson at a mass of 125 GeV with the CMS experiment at the LHC", *Phys. Lett. B* **716** (2012) 30, doi:10.1016/j.physletb.2012.08.021, arXiv:1207.7235.

[3] CMS Collaboration, "Observation of a new boson with mass near 125 GeV in pp collisions at $\sqrt{s}$ = 7 and 8 TeV", *JHEP* **06** (2013) 081, doi:10.1007/JHEP06(2013)081, arXiv:1303.4571.

[4] L. Evans and P. Bryant, "LHC machine", *JINST* **3** (2008) S08001, doi:10.1088/1748-0221/3/08/S08001.

[5] ATLAS Collaboration, "Measurement of the Higgs boson coupling properties in the $\mathrm{H} \to \mathrm{ZZ}^* \to 4\ell$ decay channel at $\sqrt{s}$ = 13 TeV with the ATLAS detector", *JHEP* **03** (2018) 095, doi:10.1007/JHEP03(2018)095, arXiv:1712.02304.

[6] CMS Collaboration, "Measurements of properties of the Higgs boson decaying into the four-lepton final state in pp collisions at $\sqrt{s} = 13$ TeV", *JHEP* **11** (2017) 047, doi:10.1007/JHEP11(2017)047, arXiv:1706.09936.

[7] ATLAS and CMS Collaborations, "Measurements of the Higgs boson production and decay rates and constraints on its couplings from a combined ATLAS and CMS analysis of the LHC pp collision data at $\sqrt{s} = 7$ and 8 TeV", *JHEP* **08** (2016) 045, doi:10.1007/JHEP08(2016)045, arXiv:1606.02266.

[8] ATLAS Collaboration, "Measurements of the Higgs boson production and decay rates and coupling strengths using pp collision data at $\sqrt{s} = 7$ and 8 TeV in the ATLAS experiment", *Eur. Phys. J. C* **76** (2016) 6, doi:10.1140/epjc/s10052-015-3769-y, arXiv:1507.04548.

[9] CMS Collaboration, "Study of the mass and spin-parity of the Higgs boson candidate via its decays to Z boson pairs", *Phys. Rev. Lett.* **110** (2013) 081803, doi:10.1103/PhysRevLett.110.081803, arXiv:1212.6639.

[10] ATLAS Collaboration, "Combined measurements of Higgs boson production and decay using up to 80 fb^{-1} of proton–proton collision data at $\sqrt{s} = 13$ TeV collected with the ATLAS experiment", ATLAS Conference Note ATLAS-CONF-2018-031, 2018.

[11] CMS Collaboration, "Combined measurements of Higgs boson couplings in proton-proton collisions at $\sqrt{s} = 13$ TeV", (2018). arXiv:1809.10733. Submitted to *EPJC*.

[12] ATLAS Collaboration, "Search for Higgs bosons decaying to *aa* in the $\mu\mu\tau\tau$ final state in pp collisions at $\sqrt{s} = 8$ TeV with the ATLAS experiment", *Phys. Rev. D* **92** (2015) 052002, doi:10.1103/PhysRevD.92.052002, arXiv:1505.01609.

[13] CMS Collaboration, "A search for pair production of new light bosons decaying into muons", *Phys. Lett. B* **752** (2016) 146, doi:10.1016/j.physletb.2015.10.067, arXiv:1506.00424.

[14] CMS Collaboration, "Search for a very light NMSSM Higgs boson produced in decays of the 125 GeV scalar boson and decaying into τ leptons in pp collisions at $\sqrt{s} = 8$ TeV", *JHEP* **01** (2016) 079, doi:10.1007/JHEP01(2016)079, arXiv:1510.06534.

[15] CMS Collaboration, "Search for light bosons in decays of the 125 GeV Higgs boson in proton-proton collisions at $\sqrt{s} = 8$ TeV", *JHEP* **10** (2017) 076, doi:10.1007/JHEP10(2017)076, arXiv:1701.02032.

[16] ATLAS Collaboration, "Search for the Higgs boson produced in association with a W boson and decaying to four b-quarks via two spin-zero particles in pp collisions at 13 TeV with the ATLAS detector", *Eur. Phys. J. C* **76** (2016) 605, doi:10.1140/epjc/s10052-016-4418-9, arXiv:1606.08391.

[17] ATLAS Collaboration, "Search for Higgs boson decays to beyond-the-Standard-Model light bosons in four-lepton events with the ATLAS detector at $\sqrt{s} = 13$ TeV", *JHEP* **06** (2018) 166, doi:10.1007/JHEP06(2018)166, arXiv:1802.03388.

[18] ATLAS Collaboration, "Search for Higgs boson decays into pairs of light (pseudo)scalar particles in the $\gamma\gamma$jj final state in pp collisions at $\sqrt{s} = 13$ TeV with the ATLAS detector", *Phys. Lett. B* **782** (2018) 750, doi:10.1016/j.physletb.2018.06.011, arXiv:1803.11145.

[19] ATLAS Collaboration, "Search for Higgs boson decays into a pair of light bosons in the bb$\mu\mu$ final state in pp collision at $\sqrt{s}$ =13 TeV with the ATLAS detector", arXiv:1807.00539. Submitted to *Phys. Lett. B*.

[20] CMS Collaboration, "Search for an exotic decay of the Higgs boson to a pair of light pseudoscalars in the final state with two b quarks and two τ leptons in proton-proton collisions at $\sqrt{s} = 13$ TeV", *Phys. Lett. B* **785** (2018) 462, doi:10.1016/j.physletb.2018.08.057, arXiv:1805.10191.

[21] CMS Collaboration, "Search for an exotic decay of the Higgs boson to a pair of light pseudoscalars in the final state of two muons and two τ leptons in proton-proton collisions at $\sqrt{s} = 13$ TeV", arXiv:1805.04865. Submitted to *JHEP*.

[22] D. Curtin et al., "Exotic decays of the 125 GeV Higgs boson", *Phys. Rev. D* **90** (2014) 075004, doi:10.1103/PhysRevD.90.075004, arXiv:1312.4992.

[23] M. Dine, W. Fischler, and M. Srednicki, "A simple solution to the strong CP problem with a harmless axion", *Phys. Lett. B* **104** (1981) 199, doi:10.1016/0370-2693(81)90590-6.

[24] J. E. Kim and H. P. Nilles, "The μ-problem and the strong CP-problem", *Phys. Lett. B* **138** (1984) 150, doi:10.1016/0370-2693(84)91890-2.

[25] U. Ellwanger, C. Hugonie, and A. M. Teixeira, "The next-to-minimal supersymmetric standard model", *Phys. Rep.* **496** (2010) 1, doi:10.1016/j.physrep.2010.07.001, arXiv:0910.1785.

[26] D. de Florian et al., "Handbook of LHC Higgs cross sections: 4. Deciphering the nature of the Higgs sector", CERN Report CERN-2017-002-M, 2016. doi:10.23731/CYRM-2017-002, arXiv:1610.07922.

[27] D. Curtin, R. Essig, and Y.-M. Zhong, "Uncovering light scalars with exotic Higgs decays to b$\bar{\text{b}}\mu^+\mu^-$", *JHEP* **06** (2015) 025, doi:10.1007/JHEP06(2015)025, arXiv:1412.4779.

[28] J. Alwall et al., "The automated computation of tree-level and next-to-leading order differential cross sections, and their matching to parton shower simulations", *JHEP* **07** (2014) 079, doi:10.1007/JHEP07(2014)079, arXiv:1405.0301.

[29] Y. Li and F. Petriello, "Combining QCD and electroweak corrections to dilepton production in FEWZ", *Phys. Rev. D* **86** (2012) 094034, doi:10.1103/PhysRevD.86.094034, arXiv:1208.5967.

[30] E. Re, "Single-top Wt-channel production matched with parton showers using the POWHEG method", *Eur. Phys. J. C* **71** (2011) 1547, doi:10.1140/epjc/s10052-011-1547-z, arXiv:1009.2450.

[31] S. Alioli, P. Nason, C. Oleari, and E. Re, "A general framework for implementing NLO calculations in shower Monte Carlo programs: the POWHEG BOX", *JHEP* **06** (2010) 043, doi:10.1007/JHEP06(2010)043, arXiv:1002.2581.

[32] S. Alioli, P. Nason, C. Oleari, and E. Re, "NLO single-top production matched with shower in POWHEG: s- and t-channel contributions", *JHEP* **09** (2009) 111, doi:10.1007/JHEP02(2010)011,10.1088/1126-6708/2009/09/111, arXiv:0907.4076.

[33] S. Frixione, P. Nason, and C. Oleari, "Matching NLO QCD computations with parton shower simulations: the POWHEG method", *JHEP* **11** (2007) 070, doi:10.1088/1126-6708/2007/11/070, arXiv:0709.2092.

[34] NNPDF Collaboration, "Parton distributions for the LHC Run II", *JHEP* **04** (2015) 040, doi:10.1007/JHEP04(2015)040, arXiv:1410.8849.

[35] T. Sjöstrand et al., "An introduction to PYTHIA 8.2", *Comput. Phys. Commun.* **191** (2015) 159, doi:10.1016/j.cpc.2015.01.024, arXiv:1410.3012.

[36] P. Skands, S. Carrazza, and J. Rojo, "Tuning PYTHIA 8.1: the Monash 2013 tune", *Eur. Phys. J. C* **74** (2014) 3024, doi:10.1140/epjc/s10052-014-3024-y, arXiv:1404.5630.

[37] CMS Collaboration, "Event generator tunes obtained from underlying event and multiparton scattering measurements", *Eur. Phys. J. C* **76** (2016) 155, doi:10.1140/epjc/s10052-016-3988-x, arXiv:1512.00815.

[38] GEANT4 Collaboration, "GEANT4—a simulation toolkit", *Nucl. Instrum. Meth. A* **506** (2003) 250, doi:10.1016/S0168-9002(03)01368-8.

[39] CMS Collaboration, "CMS luminosity measurements for the 2016 data taking period", CMS Physics Analysis Summary CMS-PAS-LUM-17-001, 2017.

[40] M. Cacciari, G. P. Salam, and G. Soyez, "The anti-k_{T} jet clustering algorithm", *JHEP* **04** (2008) 063, doi:10.1088/1126-6708/2008/04/063, arXiv:0802.1189.

[41] M. Cacciari, G. P. Salam, and G. Soyez, "FastJet user manual", *Eur. Phys. J.* **C72** (2012) 1896, doi:10.1140/epjc/s10052-012-1896-2, arXiv:1111.6097.

[42] CMS Collaboration, "Particle-flow reconstruction and global event description with the CMS detector", *JINST* **12** (2017) P10003, doi:10.1088/1748-0221/12/10/P10003, arXiv:1706.04965.

[43] CMS Collaboration, "Jet algorithms performance in 13 TeV data", CMS Physics Analysis Summary CMS-PAS-JME-16-003, 2017.

[44] CMS Collaboration, "Determination of jet energy calibration and transverse momentum resolution in CMS", *JINST* **6** (2011) P11002, doi:10.1088/1748-0221/6/11/P11002, arXiv:1107.4277.

[45] CMS Collaboration, "Identification of heavy-flavour jets with the CMS detector in pp collisions at 13 TeV", *JINST* **13** (2018) P05011, doi:10.1088/1748-0221/13/05/P05011, arXiv:1712.07158.

[46] G. Pagnini and R. K. Saxena, "A note on the Voigt profile function", (2008) arXiv:0805.2274.

[47] M. J. Oreglia, "A study of the reactions $\psi' \to \gamma\gamma\psi$". PhD thesis, Stanford University, 1980. SLAC Report SLAC-R-236.

[48] P. Dauncey, M. Kenzie, N. Wardle, and G. Davies, "Handling uncertainties in background shapes: the discrete profiling method", *JINST* **10** (2015) P04015, doi:10.1088/1748-0221/10/04/P04015, arXiv:1408.6865.

[49] CMS Collaboration, "Observation of the diphoton decay of the Higgs boson and measurement of its properties", *Eur. Phys. J. C* **74** (2014) 3076, doi:10.1140/epjc/s10052-014-3076-z, arXiv:1407.0558.

[50] ATLAS and CMS Collaborations, "Combined measurement of the Higgs boson mass in pp collisions at $\sqrt{s} = 7$ and 8 TeV with the ATLAS and CMS experiments", *Phys. Rev. Lett.* **114** (2015) 191803, doi:10.1103/PhysRevLett.114.191803, arXiv:1503.07589.

[51] F. James, "Statistical methods in experimental physics", 2nd ed., World Scientific, Singapore (2007), ISBN 9789812567956.

[52] CMS Collaboration, "Measurement of the inelastic proton-proton cross section at $\sqrt{s} = 13$ TeV", *JHEP* **07** (2018) 161, doi:10.1007/JHEP07(2018)161, arXiv:1802.02613.

[53] CMS Collaboration, "Measurements of inclusive W and Z cross sections in pp collisions at $\sqrt{s} = 7$ TeV", *JHEP* **01** (2011) 080, doi:10.1007/JHEP01(2011)080, arXiv:1012.2466.

[54] J. Butterworth et al., "PDF4LHC recommendations for LHC Run II", *J. Phys. G* **43** (2016) 023001, doi:10.1088/0954-3899/43/2/023001, arXiv:1510.03865.

[55] T. Junk, "Confidence level computation for combining searches with small statistics", *Nucl. Instrum. Meth. A* **434** (1999) 435, doi:10.1016/S0168-9002(99)00498-2, arXiv:hep-ex/9902006.

[56] A. L. Read, "Presentation of search results: the CL_s technique", *J. Phys. G* **28** (2002) 2693, doi:10.1088/0954-3899/28/10/313.

[57] G. Cowan, K. Cranmer, E. Gross, and O. Vitells, "Asymptotic formulae for likelihood-based tests of new physics", *Eur. Phys. J. C* **71** (2011) 1554, doi:10.1140/epjc/s10052-011-1554-0, 10.1140/epjc/s10052-013-2501-z, arXiv:1007.1727. [Erratum: *Eur. Phys. J. C* **73** (2013) 2501].